Macromolecules
Cite This: Macromolecules 2019, 52, 2075−2082
Article
pubs.acs.org/Macromolecules

# Mesoscopic Heterogeneity in the Curing Process of an Epoxy−Amine System

Mika Aoki,[†] Atsuomi Shundo,*[,†,‡,§] Riichi Kuwahara,[⊥] Satoru Yamamoto,[⊥] and Keiji Tanaka*[,†,‡,§,∥]

[†]Department of Applied Chemistry, [‡]Department of Automotive Science, [§]International Institute for Carbon-Neutral Energy Research (WPI-I2CNER), and [∥]Center for Future Chemistry, Kyushu University, Fukuoka 819-0395, Japan

[⊥]Dassault Systemes K. K., Tokyo 141-6020, Japan

Supporting Information

**ABSTRACT:** Epoxy resins are composed of a three-dimensional network formed by chemical reactions between epoxy and amino compounds, which plays an important role in the mechanical properties. Thus, to use epoxy resins in various applications, it is necessary to gain a better understanding of their network structure. Here, we study the structural heterogeneity evolved in an epoxy−amine mixture during the curing process on the basis of a particle tracking technique, in which the thermal motion of probe particles in the mixture was tracked, small-angle X-ray scattering measurements in conjunction with coarse-grained molecular dynamics simulation. The heterogeneous environment was generated even at the initial stage of the curing process. Notably, the characteristic length scale was on the order of several hundreds of nanometers down to several tens of nanometers, depending on the extent of curing. Once a reaction occurs between a pair of epoxy and amino groups, the temperature at the site is locally elevated due to the heat of formation, accelerating a subsequent reaction nearby. Repeating such a situation, actively and scarcely reacted domains are formed. This is the main origin of the structural heterogeneity in epoxy resins.

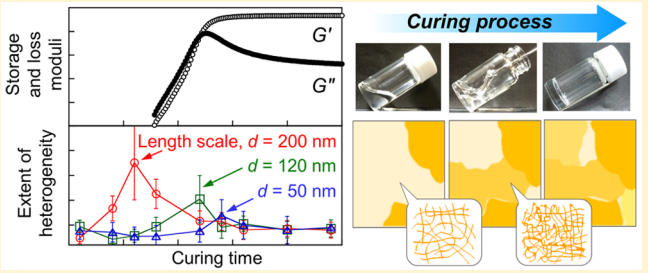


## 1. INTRODUCTION

Epoxy resins, a class of thermosetting resins, have found use in a wide range of applications such as coating agents,[1] adhesives,[2] encapsulants,[3] composites,[4,5] and so forth[6−9] thanks to their favorable mechanical properties, thermal properties, and solvent stability. Epoxy resins are based on a three-dimensional network formed via the curing reaction of epoxy and amino compounds. If one considers all of the materials that comprise the network, the network structure in epoxy resins should be related to the macroscopic mechanical properties, which play an important role in the aforementioned applications.[10−12] In fact, the mechanical properties of epoxy resins depend on the curing condition which alters how the network is formed.[13] Thus, to confer desirable properties on these resins, it is necessary to gain a better understanding of their network structure.

There are several potential approaches for characterizing the network structure. However, these may not be easily applied to epoxy resins because of their insolubility in organic solvents and infusibility at higher temperatures.[14] In general, epoxy resins are supposed to be fractured and then characterized. Scanning electron microscopy and atomic force microscopy have been commonly used for the structural analysis of thermosetting resins.[15−22] It has been reported that the nodular structure with particle sizes ranging from tens to hundreds of nanometers existed on an etched fracture surface of thermosetting resins.[15−17] A plausible explanation for the nodular structure is that it is composed of relatively higher cross-linking regions surrounded by an interstitial phase of lower cross-linking density. In this sense, the structure can be regarded as heterogeneous.[15−19] Another interpretation is that the nodular structure itself is not evidence for the presence of heterogeneity because the etched fracture surface of amorphous polymers may provide similar nodular structures.[20−22] The discrepancy between the two interpretations seems to arise from the limited number of available techniques for nondestructive characterization of the network.

Recently, small-angle neutron and X-ray scattering (SANS and SAXS, respectively) have been used to examine the network formation in the curing process of phenolic resin, which is also one of the thermosetting resins.[23−25] The swelling of the resin using a good solvent induces the spatial difference in the cross-linking density.[23] This allows for nondestructive characterization of the network mesh size and its heterogeneity. When the characteristic length scale is larger than the mesh size, however, the heterogeneity cannot be detected by scattering experiments due to it being outside the measurement range. Besides, the length scale of the heterogeneity so obtained can be difficult to compare to the one in a dried state because the resin is swollen. To gain direct

Received: November 11, 2018
Revised: February 6, 2019
Published: February 21, 2019






DOI: 10.1021/acs.macromol.8b02416
Macromolecules 2019, 52, 2075−2082

access to the mesoscopic heterogeneity, an alternative methodology for *in situ* characterization is desired.

Here, we focus on a particle tracking technique as a method for studying the network heterogeneity of an epoxy resin at the mesoscopic length scale. In this technique, probe particles are dispersed in a medium. Information on the local properties can be obtained by detecting the thermal motion of particles because the movement reflects the physical properties of the medium surrounding it.[26,27] Thus, tracking the movement of particles located at different positions can provide insights into the spatial heterogeneity in the medium.[28−31] An intriguing advantage of this technique is that the length scale of the observation can be altered by changing the particle size. In this study, we first performed a particle tracking study for the curing process of an epoxy resin. Notably, the length scale of the heterogeneity in the sample changed from several hundreds to tens of nanometers, depending on the extent of the curing. Such a change in the length scale of the heterogeneity could be associated with high and low cross-linked regions which appeared during the network formation. This picture was confirmed by coarse-grained molecular dynamics simulation (CGMD).

## 2. EXPERIMENTAL SECTION

**2.1. Materials.** Figure 1 shows chemical structures of hydrogenated bisphenol A diglycidyl ether (HDGEBA) and 1,4-

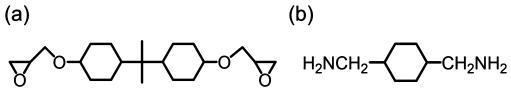


**Figure 1.** Chemical structures of (a) HDGEBA and (b) CBMA used as a precursor for epoxy resin.

cyclohexanebis(methylamine) (CBMA), which were supplied from New Japan Chemical Co., Ltd., and Tokyo Chemical Industry Co., Ltd., respectively. For the particle tracking measurements, an aqueous dispersion of polystyrene (PS) particles containing a fluorescent dye, Fluoresbrite Yellow Green Microspheres, with a concentration of 2.5 wt % was purchased from Polysciences Inc. Diameters ($d$) of particles used were 198 ± 9, 116 ± 6, and 47 ± 3 nm, denoted as 200, 120, and 50 nm, respectively. For fluorescence spectroscopy and microscopy, 4-(dimethylamino)-4′-nitrostilbene (DMANS) purchased from Tokyo Chemical Industry Co., Ltd., was used as received.

**2.2. Fourier-Transform Infrared Spectroscopy.** HDGEBA and CBMA were mixed at a molar ratio of 2:1. The mixture was sandwiched between calcium fluoride windows with a 1 mm gap. Fourier-Transform Infrared (FT-IR) spectra were recorded using a FT/IR-620 spectrometer (JASCO Co.) with a triglycine sulfate (TGS) detector. All spectra were obtained with a resolution of 2 $cm^{-1}$ and 64 scans at 296 K.

**2.3. Rheological Measurements.** Rheological measurement for the mixture of HDGEBA and CBMA was performed by an MCR 310 rheometer (Anton Paar Japan K. K.). Each of the samples was held between a sample stage and a parallel-type plate with a diameter of 8 mm. During the time-sweep measurement, strain amplitude was set to 0.1%, which was in a linear viscoelastic regime. An angular frequency was set to 10 rad $s^{-1}$, which had been commonly used to determine a gel point on the basis of the crossover point between storage ($G'$) and loss moduli ($G''$).[32] All measurements were made at 296 K.

**2.4. Particle Tracking Measurements.** A nonsticky powder of PS particles, which was obtained from the corresponding water dispersion after freeze-drying, was well dispersed into the mixture of HDGEBA and CBMA. The resultant mixture was placed in a glass bottom dish (MATSUNAMI GLASS Inc. Ltd.) and then sealed with a cover glass and vacuum grease. The moment HDGEBA and CBMA were mixed was regarded as the zero time-point. The measurements were made for a single sample after being left undisturbed at 296 K for 1, 4, 6, 8, 12, 14, 16, 20, and 24 h.

Our setup of the instrument for the particle tracking is based on an ECLIPSE Ti inverted microscope (Nikon Instech Co., Ltd.) with an N.A. 1.45 oil-immersion objective lens.[33] The bright-field observation of particles with a diameter of <200 nm was very difficult because of the light diffraction limit. Fluorescence imaging was therefore used for the measurements using smaller particles. A mercury lamp shone through an excitation filter with a passband of 460−500 nm housed in a filter block (GDP-B, Nikon Instech Co., Ltd.) illuminated the sample. Fluorescence emitted from particles went through an absorption filter with a passband of 515−560 nm in the filter block. Fluorescence images were acquired using an electron multiplying charge coupled device (EM-CCD) camera (iXon Ultra 897, Andor Technology Co., Ltd.) at a frame rate of 33 Hz. The imaging software NIS-Elements AR-4.20.00 (Nikon Instech Co., Ltd.) was used for the trajectory analysis of particles. A total of 20 different particles were individually tracked at a given curing time. The distance between particles was >30 $\mu$m. Each particle was monitored 10 times to average the diffusion behaviors.

**2.5. Small-Angle X-ray Scattering Measurements.** SAXS experiments were performed at the BL03XU beamline in SPring-8, Japan.[34] The wavelength of the incident X-rays and the sample-to-detector distance were 0.10 nm and 2230 mm, respectively. Prior to the measurement, the HDGEBA−CBMA mixture at various stages of curing was immersed in tetrahydrofuran (THF), which is a good solvent for both epoxy and amino components, at 296 K for over 48 h. The swollen or dissolved mixture was put into a quartz capillary and then installed in a sample stage. The scattered X-rays were recorded using a PILATUS 1M (DECTRIS Ltd.). By circular averaging a two-dimensional pattern on the detector, we obtained a one-dimensional scattering profile of the sample. The contribution of THF to the scattering pattern for the sample was subtracted by the pattern for pure THF, corrected using X-ray transmittance.

**2.6. Coarse-Grained Molecular Dynamics Simulations.** The question of how structural and thereby rheological heterogeneity could be formed, if at all, in the system with an ongoing curing reaction, was examined. An approach based on CGMD proposed by Okabe et al.[35,36] was adopted here for a large scale picture in 100 nm. Taking into account that the epoxy−amine reaction involves two steps, as shown in Scheme S1, we carried out the CGMD simulation. When an epoxy group approaches to within 0.6 nm of an amino group, the reaction probability $k = A \exp(-E_a/RT_l)$ is compared with a random number $P$ (0−1). Here, $A$, $E_a$, $R$, and $T_l$ are the frequency factor $A$, $1 \times 10^2$, the activation energy $E_a$, the gas constant, and the local temperature, respectively. If $k > P$, the reaction occurs, resulting in the formation of a cross-link. After the reaction, the heat of formation $\Delta H_b$ which could be estimated by increasing the kinetic energy of the part reacted, locally elevated the temperature around the reaction site. This subsequently accelerated successive reactions. Differential scanning calorimetry revealed that the activation energies for the first and second reactions in the HDGEBA-CBMA system were 56.8 and 55.3 kJ $mol^{-1}$, respectively. The $\Delta H_f$ value was fixed at 56.8 kJ $mol^{-1}$ for both reactions in this study.

The simulation was performed using Mesocite, a CGMD module of the software package Materials Studio 2018 (Dassault Systèmes K.K.). For intramolecular potentials, trajectory files of all-atom (AA) models were obtained via Forcite, a molecular dynamics module, and COMPASSII force field,[37] and then force fields for coarse-grained (CG) models were converted from the probability distributions for bond stretches, angle bends, and torsions via the Boltzmann inversion method. For intermolecular potentials, the parameters of the Lennard-Jones (LJ) potential were determined by minimizing errors between AA and CG results for the density at various temperatures.

A simulation system for the curing reaction consisted of 12962 HDGEBA and 6481 CBMA molecules using stoichiometry. A unit cell of $100 \times 100 \times 1$ $nm^3$ was used under periodic boundary conditions. After the relaxation of the system, the CGMD simulation was conducted at 296 K in the isothermal−isobaric ensemble (NPT) ensemble to reproduce the curing reaction of the epoxy resin over a


DOI: 10.1021/acs.macromol.8b02416
*Macromolecules* 2019, 52, 2075−2082

period of 2 ns. The time step was set at 10 fs, and the cross-linking reaction was judged every 10 ps.

## 3. RESULTS AND DISCUSSION

**3.1. Curing Reaction.** As a precursor for the epoxy resin, a combination of HDGEBA and CBMA was chosen because they were miscible and also reacted with each other even at room temperature. HDGEBA and CBMA were mixed at a molar ratio of 2:1, which was equivalent in stoichiometry of epoxy and amino groups. Figure 2a shows FT-IR spectra at various stages of the curing process at 296 K. For the initial stage of curing, the spectrum can be characterized by two absorption bands at 4940 and 4524 $cm^{-1}$. The former band is assignable to a combination of the stretching and bending vibrations of primary amino groups, while the latter band is due to a combination of the stretching and bending vibrations of epoxy groups.[38] With increasing curing time, the absorbance for both bands decreased, indicating that the primary amino and epoxy groups were consumed by the epoxy−amine reaction. Thus far, it has been accepted that the reaction involves different steps. A primary amino group first reacts with an epoxy group, producing a secondary amino group.[39] It again reacts with another epoxy group, resulting in the formation of a tertiary amino group, yielding a branch structure. The concentration of epoxy groups ([E]), primary ([$A_1$]), secondary ([$A_2$]), and tertiary amino groups ([$A_3$]) was estimated on the basis of the absorbance change for the bands at 4940 and 4524 $cm^{-1}$, as described in detail in the Supporting Information.[40,41] Figure 2b shows the curing time dependence of the concentrations. As the reaction proceeded, the [E] and [$A_1$] values decreased while the [$A_2$] and [$A_3$] values increased. Then, the [$A_2$] value began to decrease, while [$A_3$] kept increasing. Finally, the [$A_2$] value finally leveled off at 12 h. Thus, it seems that the chemical reaction *apparently* reached equilibrium at 12 h of curing. This was not the case, however, and this will be discussed in detail later.

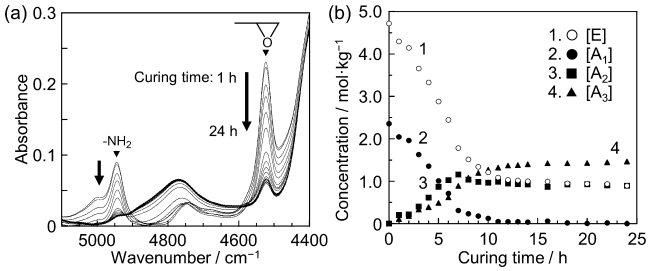


**Figure 2.** (a) FT-IR spectra for the mixture of HDGEBA and CBMA at various stages of the curing process and (b) time-dependent concentrations of functional groups.

Figure 3 shows the time dependence of storage modulus ($G'$) and loss modulus ($G''$) during the curing process at 296 K. At the initial stage of curing, although both $G'$ and $G''$ were small, $G''$ was larger than $G'$, meaning that the mixture behaved as a liquid. As curing proceeded, both $G'$ and $G''$ increased to a crossover point, 12 h, at which $G'$ and $G''$ were equal to each other, often termed a gelation time (gel point). At this point or time, the 3-dimensional network expands over the entire system.[32] After the gelation time, $G'$ asymptotically reached a constant value, while $G''$ reached a maximum shortly thereafter. Such behavior is a typical signature for vitrification. That is resin segments in between cross-linking points were frozen in mobility, leading to a less contribution of the energy dissipation.[42,43] Once the curing time exceeded 15 h, $G'$ remained unchanged. This implies that the averaged cross-linking density of the network was constant after 15 h. The curing process along with the chemical reaction and thereby the network formation was then studied using the particle tracking measurements.

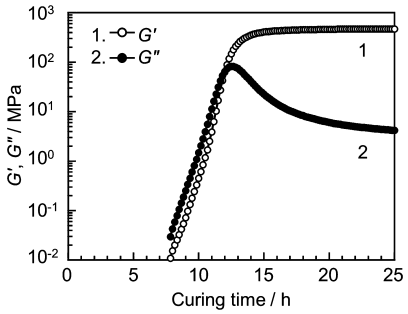


**Figure 3.** Time dependence of $G'$ and $G''$ for the HDGEBA and CBMA mixture.

**3.2. Spatial Heterogeneity.** The thermal motion of PS particles with a diameter ($d$) of 200 nm embedded in the HDGEBA−CBMA mixture was tracked. Based on the trajectory of the individual particles, mean-square displacement, $\langle \Delta r^2(t) \rangle$, is given by the equation[27]

$$\langle \Delta r^2(t) \rangle = \frac{1}{N} \sum_{i=1}^{N} \{ \mathbf{r}_i(t) - \mathbf{r}_i(0) \}^2 \quad (1)$$

where $\mathbf{r}_i(t)$ and $\mathbf{r}_i(0)$ are the positions of a particle $i$ at the lag time of $t$ and 0, and $N$ is the number of data set analyzed. The $\langle \Delta r^2(t) \rangle$ value quantitatively reflects the average travel distance of a particle from the original position after time $t$. From the slope of the double logarithmic plot of $\langle \Delta r^2(t) \rangle$ against $t$, the type of particle motion can be discussed.[27,44,45] When the slope of the plot is unity, it is apparent that the particle motion is based on the random walk statistical theory, as is commonly seen for particle diffusion in a homogeneous Newtonian fluid.[27,44] On the contrary, slopes less than 1 indicate that a particle moves in a subdiffusive manner. The subdiffusive behavior is generally explained in terms of the trapping of a particle within the aggregation structure in a material.[45]

Figure 4a shows a double-logarithmic plot of $\langle \Delta r^2(t) \rangle$ against $t$ for PS particles with $d$ = 200 nm in the HDGEBA−CBMA mixture at various stages of the curing process. Each solid line was obtained by taking an average of 10 data sets for a single particle. The slope of the hypotenuse of right-angled triangles in the figure corresponds to unity. At the initial stage of curing, and at 1 and 4 h, the slope ($n$) of all plots were equal to 1, meaning that the diffusion of particles was in accordance with the random walk statistical theory. As the reaction proceeded, the $n$ value of plots became less than 1. This indicates that the diffusion of particles was suppressed as a result of the network formation. It is noteworthy that there was a variation in the $\langle \Delta r^2(t) \rangle$ value at 6 and 8 h, suggesting the possibility that the environment surrounding probe particles was spatially heterogeneous.

In general, the length scale of the observation accessed by the particle tracking measurement is correlated to the size of probe particles used.[30,31,33,46,47] When the particle size is much larger than the characteristic length of a subject of interest, the measurement gives an insight into the bulk information which


DOI: 10.1021/acs.macromol.8b02416
Macromolecules 2019, 52, 2075−2082

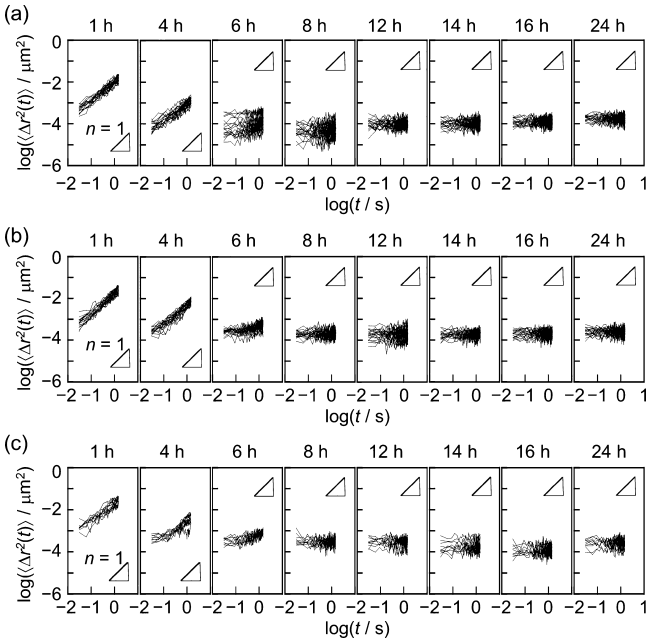


**Figure 4.** Double-logarithmic plots of $\langle \Delta r^2(t) \rangle$ against $t$ for PS particles with (a) $d$ = 200, (b) 120, and (c) 50 nm in the HDGEBA and CBMA mixture at various stages of the curing process.

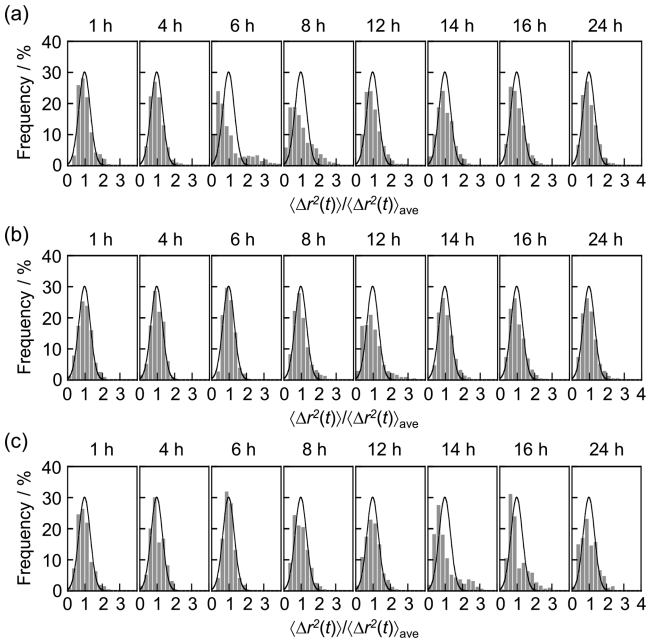


**Figure 5.** Probability distribution of the normalized $\langle \Delta r^2(t) \rangle$ values for PS particles with (a) $d$ = 200, (b) 120, and (c) 50 nm in the HDGEBA and CBMA mixture at various stages of the curing process. A solid curve in each panel denotes a fitted one, which is a Gaussian function, for PS particles in the standard homogeneous liquid glycerol.

averages variations in the local rheological properties. On the other hand, in the case of probe particles with a diameter close to or smaller than the characteristic length, the particle motion is not the same in all positions and depends on the local properties.[31,33] Hence, parallel experiments using PS particles with a diameter smaller than that used so far were performed.

Figure 4b,c shows the plot of $\langle \Delta r^2(t) \rangle$ against $t$ for PS particles with $d$ = 120 and 50 nm. The curing-induced change in the $n$ value was similar to that for particles with $d$ = 200 nm; it decreased with increasing curing time, as shown in Figure S2 of the Supporting Information. The variation in the $\langle \Delta r^2(t) \rangle$ value was also observed. However, the curing time, at which such a $\langle \Delta r^2(t) \rangle$ variation was observed, seemed to differ from that for particles with $d$ = 200 nm. To clarify such a difference, the shape of the probability distribution of $\langle \Delta r^2(t) \rangle$ normalized by the ensemble average was evaluated. To do so, all individual $\langle \Delta r^2(t) \rangle$ values at $t$ of 33 ms were divided by the mean value. When the shape can be expressed by a simple Gaussian function, or a symmetric shape, with a central value of 1, it can be claimed that the system is homogeneous in terms of its rheological properties.[30,33,48] By contrast, if a non-Gaussian distribution of the normalized $\langle \Delta r^2(t) \rangle$ values is obtained, it can be claimed that the system is heterogeneous.[29,48]

Figure 5 shows the distributions of the normalized $\langle \Delta r^2(t) \rangle$ values of particles with $d$ = 200, 120, and 50 nm at various stages of the curing process. The displacement profiles for particles with $d$ = 200 nm provided a non-Gaussian distribution at the curing times of 6 and 8 h. For particles with $d$ = 120 and 50 nm, however, the non-Gaussian distribution was obtained at later stages of the curing process. The curing times at which the non-Gaussian distribution was obtained were 12 and 14−16 h for particles with $d$ = 120 and 50 nm, respectively. Here, the non-Gaussian parameter, $\alpha_2(t)$, was calculated as follows:[49]

$$\alpha_2(t) = \frac{3\langle \Delta r^4(t) \rangle}{5\langle \Delta r^2(t) \rangle^2} - 1 \tag{2}$$

where $\langle \Delta r^4(t) \rangle$ is the fourth moment of the particle displacement. The $\alpha_2(t)$ value is a measure of the deviation from the Gaussian distribution for the particle displacement and therefore reflects the extent of the heterogeneity in the system.[30,31,45,49] A larger $\alpha_2(t)$ corresponds to more heterogeneity in the system.

Figure 6 shows the curing time dependence of $\langle \alpha_2(t) \rangle$ for particles with $d$ = 200, 120, and 50 nm. The angle brackets of

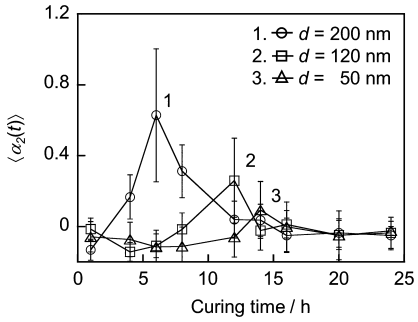


**Figure 6.** Correlation between non-Gaussian parameter $\langle \alpha_2(t) \rangle$ and curing time for PS particles with $d$ = 200, 120, and 50 nm in the HDGEBA and CBMA mixture.

$\alpha_2(t)$ denote the average over lag times, ranging from 0 to 1.5 s, where a substantial increase of $\alpha_2(t)$ with increasing $t$ was not observed. For particles with $d$ = 200 nm, the $\langle \alpha_2(t) \rangle$ value increased as the curing proceeded. Once the curing time reached 6 h, the $\langle \alpha_2(t) \rangle$ value was maximized. This makes it clear that the heterogeneity with a length scale of ∼200 nm was generated in the system after 6 h curing. With decreasing



DOI: 10.1021/acs.macromol.8b02416
Macromolecules 2019, 52, 2075−2082

particle size, the curing time showing a finite value of $\langle \alpha_2(t) \rangle$ increased. The curing times, at which $\langle \alpha_2(t) \rangle$ was maximized, were 12 and 14 h for $d$ = 120 and 50 nm, respectively. Hence, it is obvious that the length scale of the heterogeneity increased at the initial stage of curing and subsequently decreased as curing proceeded.

**3.3. Relationship between Heterogeneity and Network.** The network formation in the curing process of a phenolic resin has previously been studied by SAXS measurement with a solvent-swelling technique.[23−25] As a result, the network evolved via an interconnection of grown cross-links. A SAXS measurement was conducted to confirm whether this is the case even for the epoxy resin used here. For the sample preparation, the HDGEBA−CBMA mixtures were immersed into a good solvent, THF. The mixtures obtained at the curing time before 12 h were soluble in THF, whereas those after 12 h became insoluble due to gelation. Figure 7 shows curing time

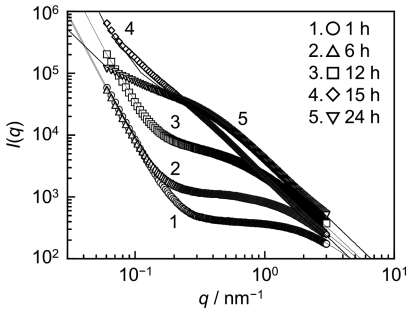


**Figure 7.** SAXS profiles for the HDGEBA−CBMA mixture in THF as solution and swollen gel states. Open symbols denote experimental data, and solid lines are the best fit curves based on a combinational scattering function of the OZ and SL equations and Porod's law.

dependence of SAXS profiles for the HDGEBA−CBMA mixture in THF. After 1 h curing, the scattering intensity was proportional to the negative fourth power of the scattering vector ($q$) in the range smaller than 0.2 nm$^{-1}$. The intensity upturn can be interpreted as Porod's law, meaning that the scattering originated from the smooth interface of domains with a relatively large size scale.[25,50,51] It therefore seems most likely that cross-linked domains appeared at the initial stage of curing.[25] As the curing reaction proceeded, the $q$ range, in which the intensity upturn was observed, shifted to a lower $q$ side. Although a quantitative discussion about the domain size cannot be undertaken at the moment, it is clear that the size of cross-linked domains increased.[25] The presence of domains at the initial stage of the curing reaction was also confirmed by fluorescence microscopic observation using a fluorescent dye based on the twisted intramolecular charge transfer (TICT), as shown in Figure S3.[52,53] The experimental data in Figure 7 could be well reproduced by combining three scattering functions such as the Ornstein−Zernike (OZ) and squared Lorentzian (SL) equations, and Porod's law, as drawn by solid lines. Curve-fitting of the data using the combinational function provided correlation lengths, $\xi$ and $\Xi$. The former is related to the average size of soluble oligomers and/or the mesh size of the network.[23,24] The latter reflects the characteristic size of heterogeneous domains.[23,24] However, the $\xi$ and $\Xi$ values obtained by the curve fitting were not the same as what is observed by our particle tracking measurement. This means that there exists the hierarchy of the heterogeneity in this mixture during the curing reaction.

Figure 8 shows a schematic illustration for the curing reaction drawn on the basis of the results shown so far. The SAXS measurements confirmed the presence of the cross-linked domains even at the initial stage of curing. In between such domains, particles embedded were expected to be sterically trapped while others in low cross-linked regions were not. This picture can explain the variation in the displacement profile for particles. Such can be seen for particles with $d$ = 200 nm after 6 h curing. Here, it should be noted that as the curing proceeded further, the $\langle \alpha_2(t) \rangle$ value for particles with $d$ = 200 nm decreased and eventually almost reached 0. Given that cross-linked domains become larger in size with increasing time, as depicted in the illustration, 200 nm particles cannot be incorporated into low cross-linked regions with a size smaller than 200 nm. Thus, 200 nm particles were insensitive to the presence of the low cross-linked regions, if any.[29,30] In other words, the size of low cross-linked regions should be <200 nm after 12 h. If that is the case, smaller particles should provide the $\langle \alpha_2(t) \rangle$ variation at the late stage of curing. This is exactly what was observed using particles with $d$ = 120 and 50 nm, as shown in Figure 6. In the case of particles with $d$ = 50 nm, $\langle \alpha_2(t) \rangle$ was maximized at 14 h, which was beyond the gel point. This means that there are low cross-linked regions with a size >50 nm even after the network expansion. A conclusive study dealing with the effects of the heterogeneity on the mechanical properties for epoxy resins will be reported in the near future.

Finally, on the basis of CGMD, the reason why such a heterogeneity appears in the curing process is discussed. Figure 9 shows CG models of HDGEBA and CBMA and the reaction conversion dependence, or time evolution, of the microstructure during the curing simulation. Each chemically connected fragment, or isolated structure, is indicated by a

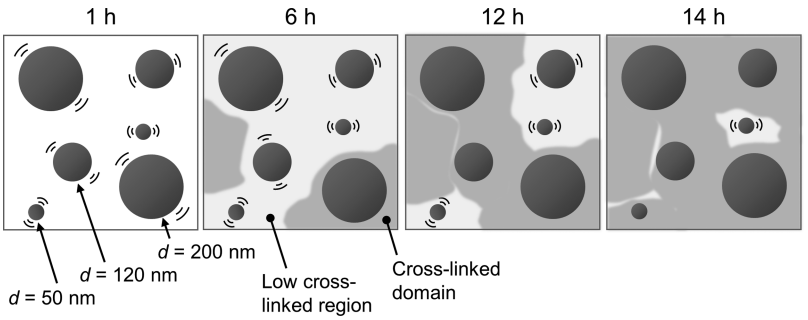


**Figure 8.** Schematic illustration showing a relationship between particle motions and network structure at various stages of the curing process. The deeper gray color represents the more cross-linked region.



DOI: 10.1021/acs.macromol.8b02416
Macromolecules 2019, 52, 2075−2082

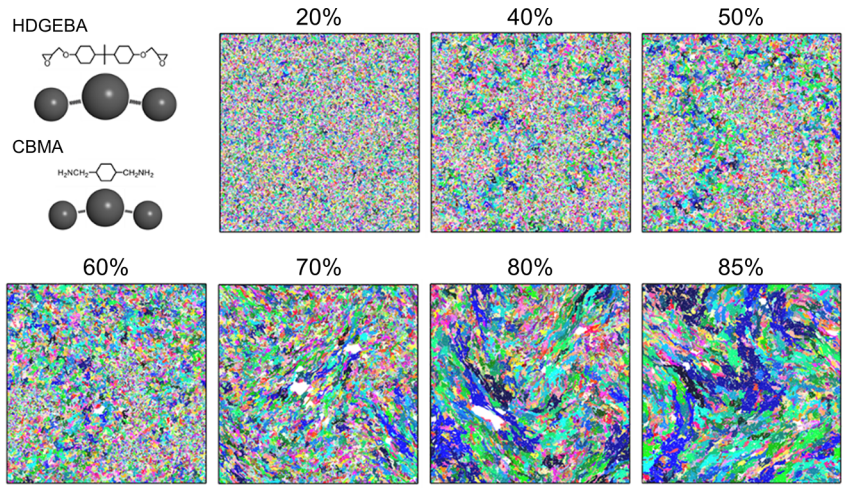


**Figure 9.** Coarse-grained models for HDGEBA and CBMA and microstructure evolution. Different colors mean each chemically connected fragment.

different color. Initial reactions were observed in spots at 20% conversion as if crystallization occurs by nucleation. They grew and fused into a larger domain with increasing conversion, resulting in the formation of a cross-linked network. At 85% conversion, the network structure was built up from many isolated fragments. In this curing process, the heterogeneity can be clearly recognized at 40−70% conversion. That is, while some regions were actively reacted, others were not. This is quite similar to what was observed in the experiment, as shown in Figure 8.

Figure 10a shows a snapshot of temperature distribution at 40% conversion with the corresponding microstructure (panel b). Superimposing the two panels, it is clear that the temperature was higher at actively reacted regions than at scarcely reacted ones. Taking into account the fact that the curing reaction is exothermic, once the reaction is initiated, subsequent reactions should be accelerated by the temperature rise, which has been caused by the heat generation of previous reactions. An additional simulation without the heat of formation revealed that the heterogeneity in the system still existed even though it was not particularly well-defined. This implies that the heterogeneity is also formed during the curing process by other factors. A possible candidate for this is the inhomogeneous propagation of reactions, which is induced by the heterogeneous diffusion of reaction points in the system, in which some regions either are or are not reacted. The heterogeneity arisen from the diffusion-controlled process is further enhanced by locally elevated temperature due to the heat of formation.

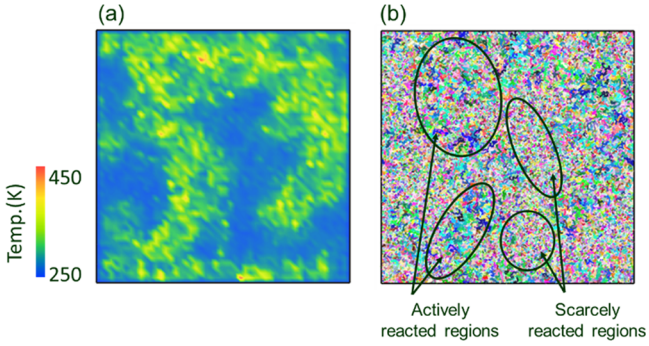


**Figure 10.** Snapshots of (a) instantaneous temperature mapping at 40% conversion and (b) corresponding microstructure with indications of actively and scarcely reacted regions.

## 4. CONCLUSIONS

A particle tracking technique was applied to the curing process of an epoxy−amine mixture, in which the network structure expanded over the entire system, resulting in an epoxy resin. The observation for individual particles at different locations, in conjunction with SAXS measurements, revealed that the mesoscopic heterogeneous structure generated even at the initial stage of the curing process, and the characteristic length scale was dependent on the curing time. This was because the heterogeneous structure was composed of actively reacted domains surrounded by scarcely reacted regions. Because the fraction of the actively and scarcely reacted regions changes with the progress of the curing reaction, the length scale of the heterogeneity depended on the curing time. CGMD clearly supported the above picture of the curing process. The two regions were formed by the reaction of functional groups, accelerated by the heat of formation generated by previous reactions. The knowledge obtained herein should be useful for understanding and controlling the mechanical properties of epoxy resins, leading to the furtherance of their functionalization. In addition, since the particle tracking technique does not require processes of physical fracture, solvent swelling, and so forth, it would be applicable to other polymer systems. Hence, we believe that both the scientific knowledge and the experimental protocol after this study will contribute to the development of functional polymer materials.

## ■ ASSOCIATED CONTENT

### Supporting Information

The Supporting Information is available free of charge on the ACS Publications website at DOI: 10.1021/acs.macromol.8b02416.

Experimental details and characterization data by FT-IR spectroscopy, particle tracking measurements, fluorescence spectroscopy, and microscopy (PDF)



DOI: 10.1021/acs.macromol.8b02416
*Macromolecules* 2019, 52, 2075−2082

## AUTHOR INFORMATION


### Corresponding Authors

*(K.T.) Tel +81-92-802-2878; e-mail k-tanaka@cstf.kyushu-u.ac.jp; fax +81-92-802-2880.
*(A.S.) Tel +81-92-802-2880, e-mail a-shundo@cstf.kyushu-u.ac.jp; fax +81-92-802-2880.

### ORCID

Atsuomi Shundo: 0000-0002-7898-3233
Keiji Tanaka: 0000-0003-0314-3843


### Notes

The authors declare no competing financial interest.

## ACKNOWLEDGMENTS

This research was partly supported by JSPS KAKENHI for Young Scientists (A) (no. JP15H05496) (A.S.) and for Scientific Research (A) (no. JP15H02183) (K.T.). We are also grateful for support from JST-Mirai Program (JPMJMI18A2) and CSTI Impulsing Paradigm Change through Disruptive Technologies (ImPACT) Program (K.T.). The synchrotron radiation facilities experiments were performed at BL03XU (Frontier Soft Matter Beamline, FSBL) in the SPring-8 with the approval of the Japan Synchrotron Radiation Research Institute (JASRI) (Proposal: 2017A7221, 2017B7273). We thank Mr. Junichiro Koike of DIC Corporation for his help in the SAXS measurements.

## REFERENCES


(1) Hao, Y.; Liu, F.; Han, E.-H. Protection of Epoxy Coatings Containing Polyaniline Modified Ultra-short Glass Fibers. *Prog. Org. Coat.* **2013**, *76*, 571−580.
(2) Prolongo, S. G.; del Rosario, G.; Ureña, A. Comparative Study on the Adhesive Properties of Different Epoxy Resins. *Int. J. Adhes. Adhes.* **2006**, *26*, 125−132.
(3) Liu, Y. Trends of Power Semiconductor Wafer Level Packaging. *Microelectron. Reliab.* **2010**, *50*, 514−521.
(4) Naebe, M.; Wang, J.; Amini, A.; Khayyam, H.; Hameed, N.; Li, L. H.; Chen, Y.; Fox, B. Mechanical Property and Structure of Covalent Functionalised Graphene/epoxy Nanocomposites. *Sci. Rep.* **2015**, *4*, 4375.
(5) Yousefi, N.; Sun, X.; Lin, X.; Shen, X.; Jia, J.; Zhang, B.; Tang, B.; Chan, M.; Kim, J.-K. Highly Aligned Graphene/polymer Nanocomposites with Excellent Dielectric Properties for High-performance Electromagnetic Interference Shielding. *Adv. Mater.* **2014**, *26*, 5480−5487.
(6) Jin, H.; Mangun, C. L.; Griffin, A. S.; Moore, J. S.; Sottos, N. R.; White, S. R. Thermally Stable Autonomic Healing in Epoxy using a Dual-microcapsule System. *Adv. Mater.* **2014**, *26*, 282−287.
(7) He, C.; Shi, S.; Wu, X.; Russell, T. P.; Wang, D. Atomic Force Microscopy Nanomechanical Mapping Visualizes Interfacial Broadening between Networks Due to Chemical Exchange Reactions. *J. Am. Chem. Soc.* **2018**, *140*, 6793−6796.
(8) Cao, S.; Li, S.; Li, M.; Xu, L.; Ding, H.; Xia, J.; Zhang, M.; Huang, K. A Thermal Self-healing Polyurethane Thermoset Based on Phenolic Urethane. *Polym. J.* **2017**, *49*, 775−781.
(9) Kakichi, Y.; Yamaguchi, A.; Hashimoto, T.; Urushisaki, M.; Sakaguchi, T.; Kawabe, K.; Kondo, K.; Iyo, H. Development of Recyclable Carbon Fiber-reinforced Plastics (CFRPs) with Controlled Degradability and Stability Using Acetal Linkage-containing Epoxy Resins. *Polym. J.* **2017**, *49*, 851−859.
(10) Kenyon, A. S.; Nielsen, L. E. Characterization of Network Structure of Epoxy Resins by Dynamic Mechanical and Liquid Swelling Tests. *J. Macromol. Sci., Chem.* **1969**, *3*, 275−295.
(11) Kishi, H.; Naitou, T.; Matsuda, S.; Murakami, A.; Muraji, Y.; Nakagawa, Y. Mechanical Properties and Inhomogeneous Nanostructures of Dicyandiamide-cured Epoxy Resins. *J. Polym. Sci., Part B: Polym. Phys.* **2007**, *45*, 1425−1434.
(12) Yamada, K.; Kishi, H. Control of Nanostructures in Epoxy/acrylic Block Copolymer Blends by The In Situ Generation of Functional Groups. *Polym. J.* **2017**, *49*, 617−623.
(13) Meyer, F.; Sanz, G.; Eceiza, A.; Mondragon, I.; Mijović, J. The Effect of Stoichiometry and Thermal History during Cure on Structure and Properties of Epoxy Networks. *Polymer* **1995**, *36*, 1407−1414.
(14) Aoki, M.; Shundo, A.; Okamoto, K.; Ganbe, T.; Tanaka, K. Segregation of an Amine Component in A Model Epoxy Resin at a Copper Interface. *Polym. J.* **2018**, DOI: 10.1038/s41428-018-0129-4.
(15) Erath, E. H.; Spurr, R. A. Occurrence of Globular Formations in Thermosetting Resins. *J. Polym. Sci.* **1959**, *35*, 391−399.
(16) Mijović, J.; Koutsky, J. A. Correlation between Nodular Morphology and Fracture Properties of Cured Epoxy Resins. *Polymer* **1979**, *20*, 1095−1107.
(17) Takahama, T.; Geil, P. H. Structural Inhomogeneities of Cured Epoxy Resins. *Makromol. Chem., Rapid Commun.* **1982**, *3*, 389−394.
(18) Gupta, V. B.; Drzal, L. T.; Adams, W. W.; Omlor, R. An Electron Microscopic Study of the Morphology of Cured Epoxy Resin. *J. Mater. Sci.* **1985**, *20*, 3439−3452.
(19) Morsch, S.; Liu, Y.; Lyon, S. B.; Gibbon, S. R. Insights into Epoxy Network Nanostructural Heterogeneity Uisng AFM-IR. *ACS Appl. Mater. Interfaces* **2016**, *8*, 959−966.
(20) Dušek, K.; Pleštil, J.; Lednický, F.; Luňák, S. Are Cured Epoxy Resins Inhomogeneous? *Polymer* **1978**, *19*, 393−397.
(21) Haba, D.; Kaufmann, J.; Brunner, A. J.; Resch, K.; Teichert, C. Observation of Elastic Modulus Inhomogeneities in Thermosetting Epoxies Using AFM-discerning Facts and Artifacts. *Polymer* **2014**, *55*, 4032−4040.
(22) Foster, S. F.; Hoff, E. A.; Curtzwiler, G. W.; Williams, E. B.; Davis, K. B.; Patton, D. L.; Rawlins, J. W. Chemorheology Investigation of a Glassy Epoxy Thermoset on Tensile Plastic Flow and Fracture Morphology. *J. Polym. Sci., Part B: Polym. Phys.* **2015**, *53*, 1333−1344.
(23) Izumi, A.; Nakao, T.; Shibayama, M. Gelation and Cross-link Inhomogeneity of Phenolic Resins Studied by $^{13}$C-NMR Spectroscopy and Small-angle X-ray Scattering. *Soft Matter* **2013**, *9*, 4188−4197.
(24) Izumi, A.; Nakao, T.; Shibayama, M. Gelation and Cross-link Inhomogeneity of Phenolic Resins Studied by Small- and Wide-angle X-ray Scattering and $^{1}$H-Pulse NMR Spectrosccopy. *Polymer* **2015**, *59*, 226−233.
(25) Izumi, A.; Shudo, Y.; Nakao, T.; Shibayama, M. Cross-link Inhomogeneity in Phenolic Resins at the Initial Stage of Curing Studied by $^{1}$H-pulse NMR Spectroscopy and Complementary SAXS/WAXS and SANS/WANS with a Solvent-swelling Technique. *Polymer* **2016**, *103*, 152−162.
(26) Valentine, M. T.; Kaplan, P. D.; Thota, D.; Crocker, J. C.; Gisler, T.; Prud'homme, R. K.; Beck, M.; Weitz, D. A. Investigating the Microenvironments of Inhomogeneous Soft Materials with Multiple Particle Tracking. *Phys. Rev. E: Stat. Phys., Plasmas, Fluids, Relat. Interdiscip. Top.* **2001**, *64*, 061506.
(27) Waigh, T. A. Microrheology of Complex Fluids. *Rep. Prog. Phys.* **2005**, *68*, 685−742.
(28) Penaloza, D. P.; Hori, K.; Shundo, A.; Tanaka, K. Spatial Heterogeneity in a Lyotropic Liquid Crystal with Hexagonal Phase. *Phys. Chem. Chem. Phys.* **2012**, *14*, 5247−5250.
(29) Tseng, Y.; Wirtz, D. Mechanics and Multiple-particle Tracking Microheterogeneity of α-Actinin-cross-linked Actin Filament Networks. *Biophys. J.* **2001**, *81*, 1643−1656.
(30) Penaloza, D. P.; Shundo, A.; Matsumoto, K.; Ohno, M.; Miyaji, K.; Goto, M.; Tanaka, K. Spatial Heterogeneity in the Sol−Gel Transition of a Supramolecular System. *Soft Matter* **2013**, *9*, 5166−5172.
(31) Matsumoto, Y.; Shundo, A.; Ohno, M.; Tsuruzoe, N.; Goto, M.; Tanaka, K. Mesoscopic Heterogeneity in Pore Size of Supramolecular Networks. *Langmuir* **2018**, *34*, 7503−7508.




DOI: 10.1021/acs.macromol.8b02416
*Macromolecules* 2019, 52, 2075−2082

(32) Tung, C.-Y. M.; Dynes, P. J. Relationship between Viscoelastic Properties and Gelation in Thermosetting Systems. *J. Appl. Polym. Sci.* **1982**, *27*, 569−574.
(33) Shundo, A.; Hori, K.; Penaloza, D. P.; Matsumoto, Y.; Okumura, Y.; Kikuchi, H.; Lee, K. E.; Kim, S. O.; Tanaka, K. Hierarchical Spatial Heterogeneity in Liquid Crystals Composed of Graphene Oxides. *Phys. Chem. Chem. Phys.* **2016**, *18*, 22399−22406.
(34) Masunaga, H.; Ogawa, H.; Takano, T.; Sasaki, S.; Goto, S.; Tanaka, T.; Seike, T.; Takahashi, S.; Takeshita, K.; Nariyama, N.; Ohashi, H.; Ohata, T.; Furukawa, Y.; Matsushita, T.; Ishizawa, Y.; Yagi, N.; Takata, M.; Kitamura, H.; Sakurai, K.; Tashiro, K.; Takahara, A.; Amamiya, Y.; Horie, K.; Takenaka, M.; Kanaya, T.; Jinnai, H.; Okuda, H.; Akiba, I.; Takahashi, I.; Yamamoto, K.; Hikosaka, M.; Sakurai, S.; Shinohara, Y.; Okada, A.; Sugihara, Y. Multipurpose Soft-material SAXS/WAXS/GISAXS Beamline at SPring-8. *Polym. J.* **2011**, *43*, 471−477.
(35) Okabe, T.; Takehara, T.; Inose, K.; Hirano, N.; Nishikawa, M.; Uehara, T. Curing Reaction of Epoxy Resin Composed of Mixed Base Resin and Curing Agent: Experiments and Molecular Simulation. *Polymer* **2013**, *54*, 4660−4668.
(36) Okabe, T.; Oya, Y.; Tanabe, K.; Kikugawa, G.; Yoshioka, K. Molecular Dynamics Simulation of Crosslinked Epoxy Resins: Curing and Mechanical Properties. *Eur. Polym. J.* **2016**, *80*, 78−88.
(37) Sun, H. COMPASS: An ab Initio Force-field Optimized for Condensed-phase Applications − Overview with Details on Alkane and Benzene Compounds. *J. Phys. Chem. B* **1998**, *102*, 7338−7364.
(38) Mijović, J.; Andjelić, S.; Kenny, J. M. In Situ Real-time Monitoring of Epoxy/amine Kinetics by Remote near Infrared Spectroscopy. *Polym. Adv. Technol.* **1996**, *7*, 1−16.
(39) Riccardi, C. C.; Adabbo, E.; Williams, R. J. J. Curing reaction of epoxy resins with diamines. *J. Appl. Polym. Sci.* **1984**, *29*, 2481−2492.
(40) Paz-Abuin, S.; Lopez-Quintela, A.; Varela, M.; Pazos-Pellín, M.; Prendes, P. Method for Determination of the Ratio of Rate Constants, Secondary to Primary Amine, in Epoxy-amine Systems. *Polymer* **1997**, *38*, 3117−3120.
(41) Hirai, T.; Kawasaki, K.; Tanaka, K. Interfacial Kinetics of a Model Epoxy−amine Addition Reaction. *Phys. Chem. Chem. Phys.* **2012**, *14*, 13532−13534.
(42) Lange, J.; Altmann, N.; Kelly, C. T.; Halley, P. J. Understanding Vitrification during Cure of Epoxy Resins Using Dynamic Scanning Calorimetry and Rheological Techniques. *Polymer* **2000**, *41*, 5949−5955.
(43) Sbirrazzuoli, N.; Vyazovkin, S.; Mititelu, A.; Sladic, C.; Vincent, L. A Study of Epoxy-amine Cure Kinetics by Combining Isoconversional Analysis with Temperature Modulated DSC and Dynamic Rheometry. *Macromol. Chem. Phys.* **2003**, *204*, 1815−1821.
(44) Oppong, F. K.; Coussot, P.; de Bruyn, J. R. Gelation on the Microscopic Scale. *Phys. Rev. E: Stat., Nonlinear, Soft Matter Phys.* **2008**, *78*, 021405.
(45) Moschakis, T.; Lazaridou, A.; Biliaderis, C. G. Using Particle Tracking to Probe the Local Dynamics of Barley $\beta$-Glucan Solutions upon Gelation. *J. Colloid Interface Sci.* **2012**, *375*, 50−59.
(46) Valentine, M. T.; Perlman, Z. E.; Gardel, M. L.; Shin, J. H.; Matsudaira, P.; Mitchison, T. J.; Weitz, D. A. Colloid Surface Chemistry Critically Affects Multiple Particle Tracking Measurements of Biomaterials. *Biophys. J.* **2004**, *86*, 4004−4014.
(47) Yamamoto, N.; Ichikawa, M.; Kimura, Y. Local Mechanical Properties of a Hyperswollen Lyotropic Lamellar Phase. *Phys. Rev. E* **2010**, *82*, 021506.
(48) Goodman, A.; Tseng, Y.; Wirtz, D. Effect of Length, Topology, and Concentration on the Microviscosity and Microheterogeneity of DNA Solutions. *J. Mol. Biol.* **2002**, *323*, 199−215.
(49) Weeks, E. R.; Weitz, D. A. Subdiffusion and the Cage Effect Studied near the Colloidal Glass Transition. *Chem. Phys.* **2002**, *284*, 361−367.
(50) Roe, R. J. *Methods of X-ray and Neutron Scattering in Polymer Science*; Oxford University Press: New York, 2000.
(51) Suzuki, D.; Nagase, Y.; Kureha, T.; Sato, T. Internal Structures of Thermosensitive Hybrid Microgels Investigated by Means of Small-Angle X-ray Scattering. *J. Phys. Chem. B* **2014**, *118*, 2194−2204.
(52) Shin, D. M.; Whitten, D. G. Solvatochromic Behavior of Intramolecular Charge-transfer Diphenylpolyenes in Homogeneous Solution and Microheterogeneous Media. *J. Phys. Chem.* **1988**, *92*, 2945−2956.
(53) Hakala, K.; Vatanparast, R.; Li, S.; Peinado, C.; Bosch, P.; Catalina, F.; Lemmetyinen, H. Monitoring of Curing Process and Shelf Life of the Epoxy-anhydride System with TICT Compounds by the Fluorescence Technique. *Macromolecules* **2000**, *33*, 5954−5959.


DOI: 10.1021/acs.macromol.8b02416
*Macromolecules* 2019, 52, 2075−2082